Published in final edited form as:

JACC Cardiovasc Imaging. 2022 March ; 15(3): 504–515. doi:10.1016/j.jcmg.2021.08.009.

Detection and Characterization of Thrombosis in Humans using Fibrin-Targeted Positron Emission Tomography and Magnetic Resonance

David Izquierdo-Garcia, PhD[1,2], **Pauline Désogère, PhD**[1,3], **Anne L. Philip**[4], **Choukri Mekkaoui, PhD**[1], **Rory B. Weiner, MD**[5], **Onofrio A. Catalano, MD**[1], **Yin-Ching Iris Chen, PhD**[1], **Doreen DeFaria Yeh, MD**[5], **Moussa Mansour, MD**[5], **Ciprian Catana, MD, PhD**[1,3], **Peter Caravan, PhD**[1,3], **David E. Sosnovik, MD**[1,3,4,5]

[1]Athinoula A. Martinos Center for Biomedical Imaging, Department of Radiology, Massachusetts General Hospital and Harvard Medical School, Charlestown, MA

[2]Harvard-MIT Department of Health Sciences and Technology, Massachusetts Institute of Technology, Cambridge, MA

[3]Institute for Innovation in Imaging, Department of Radiology, Massachusetts General Hospital

[4]Cardiovascular Research Center, Cardiology Division, Dept. of Medicine, Massachusetts General Hospital and Harvard Medical School, Boston MA

[5]Cardiology Division, Department of Medicine, Massachusetts General Hospital and Harvard Medical School, Boston, MA

Abstract

Background: The detection of thrombus in the left atrial appendage (LAA) is vital in the prevention of stroke and is currently performed using transesophageal echocardiography (TEE).

Objectives: We present a novel technique to detect and characterize LAA thrombus in humans using combined positron emission tomography-magnetic resonance imaging (PET/MRI) of a fibrin-binding radiotracer, [^{64}Cu]FBP8.

Methods: The metabolism and pharmacokinetics of [^{64}Cu]FBP8 were studied in 8 healthy volunteers. Patients with atrial fibrillation (AF) and recent TEEs of the LAA (positive n=12, negative n=12) were injected with [^{64}Cu]FBP8 and imaged with PET/MRI, including mapping the longitudinal magnetic relaxation time (T1) in the LAA .

Address for Correspondence: David Izquierdo-Garcia, 149 13th St, Suite 2301, Charlestown, MA, 02129, USA. Tel: +1-617-643-3901. Fax: +1-617-726-7422. Twitter handle: @davidizgar. Tweet: In vivo imaging of blood clots in the human heart using a novel molecular probe (#FBP8) and #PET/MRI by @davidizgar, @PeterCaravan and David Sosnovik. davidizq@nmr.mgh.harvard.edu.

Disclosures: Peter Caravan is an inventor of [^{64}Cu]FBP8 and holds intellectual property related to it. All other authors declare no conflicts of interest.

Results: [^{64}Cu]FBP8 was stable to metabolism and was rapidly eliminated. The maximum standardized uptake value (SUV_{Max}) in the LAA was significantly higher in the TEE positive than negative subjects, median [interquartile range] of 4.0 [3.0-6.0] vs. 2.3 [2.1-2.5]; $p < 0.001$, with an area-under-the-receiver operating characteristic curve of 0.97. A SUV_{Max} threshold of 2.6 provided a sensitivity of 100% and specificity of 84%. The minimum T1 ($T1_{Min}$) in the LAA was 970ms [780-1080] vs. 1380ms [1120-1620] (TEE positive vs. negative), $p < 0.05$, with some overlap between the groups. Logistic regression using SUV_{Max} and $T1_{Min}$ allowed all TEE positive and negative subjects to be classified with 100% accuracy.

Conclusion: PET/MR of [^{64}Cu]FBP8 is able to detect acute as well as older platelet-poor thrombi with excellent accuracy. Furthermore, the integrated PET/MRI approach provides useful information on the biological properties of thrombus such as fibrin and methemoglobin content.

Clinical Trial: Imaging of LAA Thrombosis URL: https://clinicaltrials.gov/ct2/show/NCT03830320 Registration number: NCT03830320

Keywords

Atrial fibrillation; thrombus; PET; MRI; fibrin; left atrial appendage

Introduction

Thrombosis plays a central role in numerous cardiovascular diseases (1). While major advances have been made in the molecular understanding and treatment of thrombosis, its diagnosis remains indirect and imprecise (2,3). The presence of a filling defect on computed tomography (CT) and magnetic resonance imaging (MRI), or the detection of echogenic material on ultrasound, currently form the basis of non-invasive thrombus detection. These approaches are of major clinical utility but provide no information on the molecular and cellular properties of the thrombus. In addition, these techniques frequently employ nephrotoxic contrast agents, have limited anatomical coverage and, in the case of transesophageal echo (TEE), involve heavy sedation and the risk of esophageal trauma.

A number of molecular imaging approaches targeting platelets (4,5), fibrin (6,7), d-dimers (8,9), or fibrinogen (10), have been proposed, with some progressing to clinical trials (3,11). However these agents have been limited by suboptimal pharmacokinetics, high blood background, low specificity, or sensitivity only to hyperacute/acute thrombi (3). We and others have previously described the use of a small fibrin-avid peptide to image thrombosis by MRI (6,12,13). The translational potential of this agent (EP-2104R), however, was limited at the time due to concerns regarding the potential toxicity of gadolinium (14,15). While these concerns have not materialized, and no toxicity from EP-2104R has emerged, it did motivate us to design a new agent with a less complicated pathway towards clinical translation.

We have recently reported the preclinical development of a small peptide based fibrin-specific probe labeled with the copper-64 isotope to detect thrombus by positron emission tomography (PET) (16). This probe, [^{64}Cu]FBP8, has submicromolar affinity for fibrin, and facilitated the rapid detection of venous, arterial, and embolic thrombi in a number of

animal models (16–18). Here, we report the first human experience with [^{64}Cu]FBP8, which we use to detect left atrial appendage (LAA) thrombus in subjects with atrial fibrillation (Afib). The detection of LAA thrombus was selected due to the clinical prevalence of Afib and stroke (19), because TEE provides an accurate gold standard for comparison (20), and because the use of LAA occlusion devices in selected individuals allows the development of the thrombus to be precisely timed (21,22). We further aimed in the study to assess whether an integrated PET/MRI approach, enabling the simultaneous acquisition of PET and longitudinal magnetic relaxation (T1) maps of the heart would enhance diagnostic accuracy and help characterize the detected thrombi.

Methods

Study Subjects

This study was approved by the Mass General Brigham (MGB) Institutional Review Board (protocol number 2015P002385) and registered on the ClinicalTrials.gov website (NCT03830320). All subjects were aware of the benefits/risks of the study and provided written consent. Healthy controls (HC) were recruited via the MGB Research Study Volunteer Program, and had to be 18 years of age or older with no known medical issues, have no history of Afib or thrombosis, and a negative drug screen. Patients with Afib, presenting to the electrophysiology laboratory at the Massachusetts General Hospital (MGH) for TEE guided cardioversion, were recruited for the LAA arm of the study. These subjects fell into three groups: those with no sign of LAA thrombus in the TEE (n=12), those with spontaneous thrombi in the LAA on TEE (n=4), and those in whom thrombus in the LAA was purposefully induced through the placement of a LAA closure device (Watchman, Boston Scientific, n=8). Most of the subjects (7/8) with Watchman devices were imaged within 12 days of the device being placed. One Watchman subject was recruited from the echocardiography laboratory at the MGH when presenting for his scheduled TEE 6 weeks after the placement of the device. All subjects underwent PET/MRI with [^{64}Cu]FBP8 within 14 days of their reference TEE. Subjects were excluded if they had electrical implants such as a cardiac pacemaker/defibrillator, exceeded the weight limit of the PET/MRI scanner or had a contraindication to MRI. Further details on the clinical characteristics of the TEE negative and TEE positive study subjects are provided in Table 1 and in the supplement. The synthesis of [^{64}Cu]FBP8 and the chemical analysis of blood samples are also described in the supplement.

PET/MRI Data Acquisition

All images were acquired on a simultaneous PET/MRI scanner (Biograph mMR, Siemens Heathineers, USA) at a single station (~45 min) for the Afib subjects and at multiple stations (~ 2h) for the HCs. For all subjects, PET images were retrospectively reconstructed around 70 min post injection of approximately 380 and 250 MBq of [^{64}Cu]FBP8 for the HC and Afib subjects respectively. Simultaneously to the PET imaging, the following MRI sequences were acquired: a dual-echo Dixon-VIBE and HASTE sequences (both HC and Afib), and ECG-gated balanced steady state free precession (bSSFP) cine images and Modified Look-Locker imaging (MOLLI) sequences for Afib subjects only.

PET Image Analysis

Signal was measured in two regions of interest (ROIs) in the PET images: The LAA and the left ventricular blood pool. To avoid bias, the ROIs were drawn using OsiriX MD (v. 10.3, Pixmeo, Switzerland) on the T2 Haste images (HC) or the Dixon opposite phase images (Afib subjects) and then copied without modification to the PET images. A large spherical ROI was drawn to enclose the entire LAA and was standardized as much as possible across the subjects.

PET images were converted into standardized uptake values (SUV) using the subject's weight as a normalization factor (23). Mean and maximum SUVs (SUV and SUV_{MAX} respectively) were obtained from the ROIs after exporting the OsiriX ROIs into Matlab for data analysis. Receiver operating characteristic (ROC) analysis of the SUV_{MAX} values was performed in GraphPad Prism and a SUV_{MAX} threshold of 2.6 was chosen from the ROC curve to provide 100% sensitivity.

T1 Map Analysis

T1 maps were produced using the reconstruction package provided by the manufacturer (Myomaps, Siemens Healthineers). ROIs were drawn using OsiriX in each coronal and axial T1 map in the three following regions: 1) LAA, a manually drawn ROI that closely followed the anatomical contour of the LAA; 2) $BloodPool_{T1}$, a manually drawn ROI in either the left atrium or the right pulmonary artery; 3) *Fat*, a subcutaneous fat ROI near the LAA. ROIs were exported into an in-house Matlab program and mean and minimum T1 values (T1 and $T1_{min}$ respectively) were obtained from the LAA. To prevent voxels within the adipose tissue surrounding the LAA from biasing the analysis, voxels within the LAA with values lower than two standard deviations above the mean of the *Fat* region were excluded.

Combined PET/MRI Analysis: Z-Score Analysis with Logistic Regression

Z-scores are defined as the number of standard deviations above (for PET images) or below (for T1 maps) the mean of the background region, as follows:

$$Z_{PET} = \frac{SUV_{max} - \overline{BloodPool}}{SD_{BloodPool}}, \quad Z_{T1} = \frac{\overline{BloodPool_{T1}} - T1_{min}}{SD_{BloodPool_{T1}}}$$

Z-scores for PET and T1 were used in a logistic regression analysis to estimate the predictive probability of combined PET and MR measurements to define a subject i as positive/negative, with respect to the gold standard of TEE, as follows:

$$p_i = \frac{e^{\beta_0 + \beta_1 \cdot Z^i_{PET} + \beta_2 \cdot Z^i_{MR}}}{1 + e^{\beta_0 + \beta_1 \cdot Z^i_{PET} + \beta_2 \cdot Z^i_{MR}}}$$

Qualitative Analysis

Qualitative analysis of the PET images, identifying a patient as positive or negative for increased FBP8 uptake over the LAA, was performed by a radiologist with more than

15y of experience (O.C.), who was blinded to the TEE data. Due to the heterogeneous elimination of the probe from the blood pool, images were individually windowed to produce a consistent appearance of the left ventricular blood pool.

Statistical Analysis

Descriptive statistics were calculated to summarize clinical characteristics. Differences between the TEE positive and negative groups were assessed using a two-tailed Student's t-test for normally distributed characteristics, and a Mann-Whitney test for non-normally distributed characteristics. A Fisher's exact test (with Freeman-Halton extension for multiple comparisons) was used for dichotomous outcomes. All datasets were tested for normality (GraphPad Prism) using the D'Agostino-Pearson omnibus K2 test. The maximum SUV value (SUV_{MAX}) in the LAA of the TEE positive and negative subjects was compared using a Mann-Whitney test (GraphPad Prism). The minimum T1 value ($T1_{MIN}$) in the LAA of the TEE positive and negative subjects was also compared using a Mann-Whitney test (GraphPad Prism). Median values with interquartile ranges are reported for both SUV_{MAX} and $T1_{MIN}$. Correlations were calculated using the Spearman coefficient. Logistic regression was used, as explained above, to estimate the predictive probability of the combined PET/MRI measurements, using the *predict* and *GLM* functions in R with a binomial family. All statistical tests were run on Graphpad Prism v.8.4.0 or Rstudio v.1.2 using R package v.3.6.2.

Results

Safety and Pharmacokinetics of [^{64}Cu]FBP8 in Healthy Human Volunteers

The pharmacokinetics of [^{64}Cu]FBP8, the structure of which is provided in Figure 1A, were highly consistent. The relatively low molecular weight of 2300 Da facilitated rapid and efficient excretion into the urine (Figure 1B). A smaller fraction of the radioactivity was excreted via the hepatobiliary system. Time activity curves (TACs) from ROIs drawn in the left ventricle (blood pool), lung, and background (measured in a large ROI capturing the gluteus maximus and/or the quadriceps muscles) showed that [^{64}Cu]FBP8 was rapidly cleared from these tissues (Figure 1B), with little activity remaining by 4 hours. High performance liquid chromatography (HPLC), metabolite analysis, binding activity results are shown in Figure 1C–1F. A visual depiction of [^{64}Cu]FBP8 biodistribution is provided in Figure 1G, and a magnified view of the heart in Figure 1H. The background signal in the heart and thorax was low within 1 hour of injection and was virtually eliminated within 4 hours of injection (see supplement).

Comparison of [^{64}Cu]FBP8 versus TEE in Subjects with Atrial Fibrillation

The characteristics of the subjects in the TEE positive and negative cohorts are described in the Table 1. The majority (21/24) of subjects were taking direct oral anticoagulants (DOACs) at the time of imaging, 2 were taking warfarin and 1 was not taking any anticoagulant. Five of the subjects in the TEE positive group, and one in the TEE negative group, had a history of TIA, stroke or thromboembolism. One of the subjects in the study (in the TEE negative group) had a history of a hypercoagulable state (Factor V Leiden).

The [^{64}Cu]FBP8 images in the TEE positive patients typically showed a region of high focal uptake in the LAA compared to the PET signal in the rest of the blood pool and the surrounding tissue. This is shown in Figure 2A–F, where several spontaneous thrombi are present in the LAA by TEE. PET imaging with [^{64}Cu]FBP8 detected all of these thrombi. Foci of intense [^{64}Cu]FBP8 uptake were detected in the LAA of all the TEE positive patients. In contrast, the majority of TEE negative subjects showed no evidence of focal [^{64}Cu]FBP8 uptake in the LAA. This is well demonstrated in Figure 2G–I in a subject with spontaneous echo contrast (SEC) but no thrombus within the LAA. The maximum standardized uptake values (SUV_{MAX}) in the LAA were significantly higher in the TEE positive than TEE negative group (median and interquartile range of 4.0 [3.0-6.0] vs. 2.3 [2.1-2.5]; $p < 0.001$). A SUV_{MAX} threshold of 2.6 yielded a sensitivity of 100% and specificity of 84% (Figure 2J–K). ROC analysis of SUV_{MAX} produced an area-under-the-ROC-curve (AUROC) of 0.97 (Figure 2L).

The LAA thrombi induced by the placement of the occlusion device (Watchman, Boston Scientific) were extremely conspicuous (Central Illustration), likely reflecting the size and high fibrin content in these thrombi. The majority of the Watchman subjects (7/8) were imaged 5-12 days after the procedure. The other Watchman subject was imaged at day 54 and the thrombus in the LAA remained extremely conspicuous (SUV_{MAX} of 7.9). All thrombi in the Watchman subjects were confined to the LAA, behind the device, and no evidence of communication between the LAA and left atrium was seen on the bSSFP cine images.

Integrated Approach with [^{64}Cu]FBP8 PET and MR T1 Mapping

Inspection of the individual T1 weighted images in the TEE positive subjects frequently revealed the presence of hyperintense signal in the LAA (Figure 3A, 3E), consistent with LAA thrombus. T1 mapping confirmed the presence of large foci of reduced T1 in the LAA, which were extremely conspicuous in the Watchman subjects (Figure 3B–C). Quantitative analysis of the T1 maps showed that $T1_{MIN}$ in the LAA was significantly shorter in the TEE positive subjects compared to the TEE negative subjects 970 [780-1080] versus 1380 [1120-1620], respectively, $p < 0.05$; although there was some overlap in the $T1_{MIN}$ values between the groups. Joint analysis of the SUV and T1 data was then performed using logistic regression. Logistic regression using the combined z-scores of SUV_{MAX} and $T1_{MIN}$ as inputs was extremely accurate (Figure 3J). All TEE positive cases were detected with a probability of 100% and no TEE negative case had a probability > 30%. The diagnostic accuracy of this approach was 100%, with an AUROC of 1.

The relationship between fibrin and methemoglobin (met-heme) content in the LAA, measured by SUV_{MAX} and $R1_{MAX}$ ($1/T1_{MIN}$), respectively, was complex. The correlation between these measures in spontaneous LAA thrombi was poor, perhaps reflecting the heterogeneous nature of this group. However, in the remaining 14 subjects in whom both SUV and R1 data were available (8 Watchman and 6 TEE negative) a strong correlation ($r = 0.76$) was seen between fibrin and met-heme content in the LAA (Figure 3K). Further, in the 6 TEE negative subjects, the presence of both high SUV_{MAX} and $R1_{MAX}$ values in the LAA

was associated with high risk features, such as a Factor V Leiden mutation and a history of cerebral thromboembolism (Figure 3L).

Composite Detection of Cardiac and Extracardiac Thrombi

While quantitative analysis with the SUV_{MAX} threshold described above produced a sensitivity of 100%, qualitative inspection of the images correctly classified 11/12 TEE positive subjects and 12/12 TEE negative subjects. Co-incidental thrombi were relatively uncommon and included 1 pulmonary embolism (Figure 4A–C) and right atrial appendage thrombus in 4/24 subjects.

Discussion

Anticoagulation is recommended in many clinical scenarios but is frequently empiric and complicated by the risk of major, and potentially fatal, hemorrhage (1,2). We show in this first-in-human study that PET/MRI of the fibrin-binding PET probe [^{64}Cu]FBP8 can detect acute to subacute LAA thrombi with a sensitivity of 100% and specificity of 84%, matching the performance of current more invasive approaches. The probe allows the composite burden of arterial thrombosis and venous thrombi, particularly those in larger veins with the potential to embolize, to be imaged and could potentially play a valuable role in elucidating the source of embolism in patients with TIAs and stroke, although this needs to be validated with further studies. The integrated PET/MRI approach also provides specific signatures that directly reflect the biological properties of the thrombus.

Human thrombus molecular imaging has been attempted in the past with limited success (3,9,10). The development and application of [^{64}Cu]FBP8 was based on the rational design of its preclinical precursors (16–18), and prior human studies with a fibrin-binding MR-detectable agent, EP-2104R (6). While no cases of nephrogenic systemic fibrosis have been reported with EP-2104R, the use of gadolinium-based probes in subjects with renal impairment remains a concern. In addition, the imaging of EP-2104R frequently involved two separate MRI sessions for pre- and post-contrast imaging, although post-contrast imaging alone may be sufficient (13), particularly with newer approaches such as T1 mapping. A strong case existed, therefore, to develop a PET-based probe based on the fibrin-binding peptide in EP-2104R. [^{64}Cu]FBP8 emerged from this process with nanomolar affinity to fibrin, rapid blood clearance, absence of metabolism in rodents, and high sustained and specific uptake in different animal models of arterial, venous, and embolic thrombi (17,18).

Many targets that have been explored for thrombus detection are highly expressed in acute but not chronic thrombi. The $glycoprotein_{IIb/IIIa}$ receptor, for instance, is only suited to the detection of acute platelet-rich thrombi (4). While the level of fibrin in thrombi does decrease with time (18), our data suggest that it remains sufficient to support detection with [^{64}Cu]FBP8 for at least 8-10 weeks. We estimate based on serial TEEs that one of the spontaneous thrombi detected in the study may have been up to 9 weeks old. In addition, one of the subjects with a Watchman device was imaged 54 days after implantation. The SUVs in the thrombi over this range (< 10 weeks) remained stable. Further study will be needed to determine the sensitivity of [^{64}Cu]FBP8 for chronic thrombi (> 10 weeks), the utility of

adding a gadolinium-based contrast agent to facilitate their detection, and the embolic risk of these fibrin-poor organized thrombi.

The degradation of red blood cells in subacute thrombi results in the production of the strongly paramagnetic met-heme species, which can be detected with T1 mapping (24). When integrated with PET imaging of [^{64}Cu]FBP8, the combined approach detected the presence or absence or thrombus with 100% accuracy. In addition, relevant biological information on the properties of the thrombus could be obtained (24). In large acute to subacute thrombi (Watchman subjects), and interestingly in the TEE negative subjects as well, a strong correlation was seen between fibrin and met-heme content in the LAA. High SUV_{MAX} and $R1_{MAX}$ values in the TEE negative subjects were also associated with high-risk features such as the presence of a hypercoagulable state (Factor V Leiden) or history of cerebral thromboembolism. While very preliminary, these observations raise the possibility that small microthrombi, undetectable by TEE, may be present in the LAA during Afib (25). Studies using transorbital Doppler in TEE negative subjects have documented multiple embolic signals to the brain, supporting this concept. In subjects with spontaneous LAA thrombi the correlation between fibrin and met-heme content in the thrombus was poor. This likely represents the heterogeneous nature of this cohort and the older age of their thrombi. Collectively, while very preliminary, the observations above demonstrate the potential value of integrated PET/MRI imaging with [^{64}Cu]FBP8, T1 mapping and other forms of endogenous MR contrast (magnetization transfer, diffusion) with sensitivity to thrombi (26).

Study Limitations

The PET images of [^{64}Cu]FBP8 were not gated or motion corrected, which could result in volume averaging and the underestimation of probe uptake. Although we minimized potential artifacts introduced by the attenuation correction method supplied by the scanner manufacturer, remaining inaccuracies could have biased our measurements. The pharmacokinetic studies in healthy volunteers indicated that imaging of [^{64}Cu]FBP8 should ideally be performed 4 hours after injection. However, for logistical reasons, imaging in this study was performed 1 hour after probe injection. Since the rate of renal excretion of the probe varies significantly, this resulted in heterogeneous levels of background/blood pool signal both within and between the healthy controls and the TEE groups. However, despite the higher background signal, the LAA thrombi were highly conspicuous with high thrombus to background ratios. The number of spontaneous LAA thrombi in the study was low but sufficient, we believe, to demonstrate proof-of-principle in this first-in-human study. Further studies will be required to validate our results in larger prospective clinical trials.

Conclusions

We present the first human experience with a novel fibrin-binding radiotracer, [^{64}Cu]FBP8, and show that it facilitates the detection of acute-subacute LAA thrombi with a sensitivity of 100% and a diagnostic accuracy greater than 90%. We also show that the integrated use of [^{64}Cu]FBP8 and T1 mapping of the LAA can further increase diagnostic accuracy and characterize aspects of thrombus biology. The probe is well

tolerated, demonstrates favorable pharmacokinetics and can support whole body detection of thrombosis. [^{64}Cu]FBP8 has the potential to advance the understanding of thrombus biology and to transform the diagnosis and treatment of thrombosis in a wide range of disease settings.

Supplementary Material

Refer to Web version on PubMed Central for supplementary material.

Acknowledgments:

We thank the members of the radiopharmacy laboratory at the Martinos Center for their assistance in the preparation of [^{64}Cu]FBP8. We thank the nurses and physicians in the electrophysiology laboratory at the MGH for their co-operation in subject recruitment. We thank the PET/MRI technologists in the Martinos Center for their assistance.

Funding:

Support for this study was provided in part by the following grants from the National Institutes of Health: R01HL109448 (PC and DES), R01HL141563 (DES), R01HL131907 (PC), R01HL131635 (CM), R01CA218187 (CC), and the following grants to the A. A. Martinos Center for Biomedical Imaging: S10RR022976, S10RR019933, P41EB015896.

Abbreviation list:

PET/MRI	Positron emission tomography / Magnetic resonance imaging
TEE	Transesophageal echocardiography
LAA	Left atrial appendage
HC	Healthy Controls
Afib	Atrial fibrillation
ECG	Electrocardiogram
ROI	Region of interest
SUV	Standardized uptake values
ROC	Receiver operating characteristic curve
TACs	Time activity curves
SEC	spontaneous echo contrast
bSSFP	balanced steady state free precession

References

1. Wendelboe AM, Raskob GE. Global Burden of Thrombosis: Epidemiologic Aspects. Circ Res 2016;118:1340–7. [PubMed: 27126645]
2. Tritschler T, Kraaijpoel N, Le Gal G, Wells PS. Venous Thromboembolism: Advances in Diagnosis and Treatment. JAMA 2018;320:1583–1594. [PubMed: 30326130]

3. Lanza GM, Cui G, Schmieder AH et al. An unmet clinical need: The history of thrombus imaging. J Nucl Cardiol 2019;26:986–997. [PubMed: 28608182]
4. Chae SY, Kwon TW, Jin S et al. A phase 1, first-in-human study of (18)F-GP1 positron emission tomography for imaging acute arterial thrombosis. EJNMMI Res 2019;9:3. [PubMed: 30617563]
5. Cui G, Akers WJ, Scott MJ et al. Diagnosis of LVAD Thrombus using a High-Avidity Fibrin-Specific (99m)Tc Probe. Theranostics 2018;8:1168–1179. [PubMed: 29464007]
6. Botnar RM, Perez AS, Witte S et al. In vivo molecular imaging of acute and subacute thrombosis using a fibrin-binding magnetic resonance imaging contrast agent. Circulation 2004;109:2023–9. [PubMed: 15066940]
7. Bautovich G, Angelides S, Lee FT et al. Detection of deep venous thrombi and pulmonary embolus with technetium-99m-DD-3B6/22 anti-fibrin monoclonal antibody Fab' fragment. J Nucl Med 1994;35:195–202. [PubMed: 8294982]
8. Macfarlane D, Socrates A, Eisenberg P et al. Imaging of deep venous thrombosis in patients using a radiolabelled anti-D-dimer Fab' fragment (99mTc-DI-DD3B6/22-80B3): results of a phase I trial. Eur J Nucl Med Mol Imaging 2009;36:250–9. [PubMed: 18800218]
9. Morris TA, Marsh JJ, Konopka R, Pedersen CA, Chiles PG. Improved imaging of deep venous thrombi during anticoagulation using radiolabelled anti-D-dimer antibodies. Nucl Med Commun 2004;25:917–22. [PubMed: 15319597]
10. Lensing AW, Hirsh J. 125I-fibrinogen leg scanning: reassessment of its role for the diagnosis of venous thrombosis in post-operative patients. Thromb Haemost 1993;69:2–7. [PubMed: 8446932]
11. Oliveira BL, Caravan P. Peptide-based fibrin-targeting probes for thrombus imaging. Dalton Trans 2017;46:14488–14508. [PubMed: 29051933]
12. Kolodziej AF, Nair SA, Graham P et al. Fibrin specific peptides derived by phage display: characterization of peptides and conjugates for imaging. Bioconjug Chem 2012;23:548–56. [PubMed: 22263840]
13. Spuentrup E, Botnar RM, Wiethoff AJ et al. MR imaging of thrombi using EP-2104R, a fibrin-specific contrast agent: initial results in patients. European Radiology 2008;18:1995–2005. [PubMed: 18425519]
14. Guo BJ, Yang ZL, Zhang LJ. Gadolinium Deposition in Brain: Current Scientific Evidence and Future Perspectives. Frontiers in Molecular Neuroscience 2018;11:1–12. [PubMed: 29403353]
15. Turyanskaya A, Rauwolf M, Pichler V et al. Detection and imaging of gadolinium accumulation in human bone tissue by micro- and submicro-XRF. Scientific Reports 2020;10:6301–6301. [PubMed: 32286449]
16. Ay I, Blasi F, Rietz TA et al. In vivo molecular imaging of thrombosis and thrombolysis using a fibrin-binding positron emission tomographic probe. Circ Cardiovasc Imaging 2014;7:697–705. [PubMed: 24777937]
17. Blasi F, Oliveira BL, Rietz TA et al. Radiation Dosimetry of the Fibrin-Binding Probe (6)(4)Cu-FBP8 and Its Feasibility for PET Imaging of Deep Vein Thrombosis and Pulmonary Embolism in Rats. J Nucl Med 2015;56:1088–93. [PubMed: 25977464]
18. Blasi F, Oliveira BL, Rietz TA et al. Multisite Thrombus Imaging and Fibrin Content Estimation With a Single Whole-Body PET Scan in Rats. Arterioscler Thromb Vasc Biol 2015;35:2114–21. [PubMed: 26272938]
19. Wolf PA, Abbott RD, Kannel WB. Atrial fibrillation as an independent risk factor for stroke: the Framingham Study. Stroke 1991;22:983–8. [PubMed: 1866765]
20. Manning WJ, Weintraub RM, Waksmonski CA et al. Accuracy of transesophageal echocardiography for identifying left atrial thrombi. A prospective, intraoperative study. Ann Intern Med 1995;123:817–22. [PubMed: 7486462]
21. Holmes DR Jr., Reddy VY, Gordon NT et al. Long-Term Safety and Efficacy in Continued Access Left Atrial Appendage Closure Registries. J Am Coll Cardiol 2019;74:2878–2889. [PubMed: 31806131]
22. Hucker WJ, Cohen JA, Gurol ME et al. WATCHMAN implantation in patients with a history of atrial fibrillation and intracranial hemorrhage. J Interv Card Electrophysiol 2019.
23. Izquierdo-Garcia D, Davies JR, Graves MJ et al. Comparison of methods for magnetic resonance-guided [18-F]fluorodeoxyglucose positron emission tomography in human carotid arteries:

reproducibility, partial volume correction, and correlation between methods. Stroke; a journal of cerebral circulation 2009;40:86–93.

24. Saha P, Andia ME, Modarai B et al. Magnetic resonance T1 relaxation time of venous thrombus is determined by iron processing and predicts susceptibility to lysis. Circulation 2013;128:729–736. [PubMed: 23820077]
25. Higuchi E, Toi S, Shirai Y et al. Prevalence of Microembolic Signals in Embolic Stroke of Undetermined Source and Other Subtypes of Ischemic Stroke. Stroke 2020;51:655–658. [PubMed: 31771457]
26. Phinikaridou A, Andia ME, Saha P, Modarai B, Smith A, Botnar RM. In vivo magnetization transfer and diffusion-weighted magnetic resonance imaging detects thrombus composition in a mouse model of deep vein thrombosis. Circ Cardiovasc Imaging 2013;6:433–440. [PubMed: 23564561]

Clinical Perspectives

Clinical Competency

Medical Knowledge

- The presence of fibrin in thrombus allow both acute and older thrombi to be detected by positron emission tomography (PET)
- Mapping the longitudinal relaxation time (T1) in the left atrial appendage (LAA) may allow thrombi to be detected via a reduction in T1

Translational Outlook

- Serial imaging with [^{64}Cu]FBP8 could be used to better understand the natural history of thrombus in the cardiovascular system
- The detection of LAA thrombus with [^{64}Cu]FBP8 could be used to refine the risk for thrombo-embolism in those at high risk of anticoagulation.
- [^{64}Cu]FBP8 could play a valuable role in detecting the source of embolism/thrombus in those with transient ischemic attacks and stroke
- The presence of high fibrin levels ([^{64}Cu]FBP8 uptake) in a thrombus could be used to predict the likelihood of successful thrombolysis

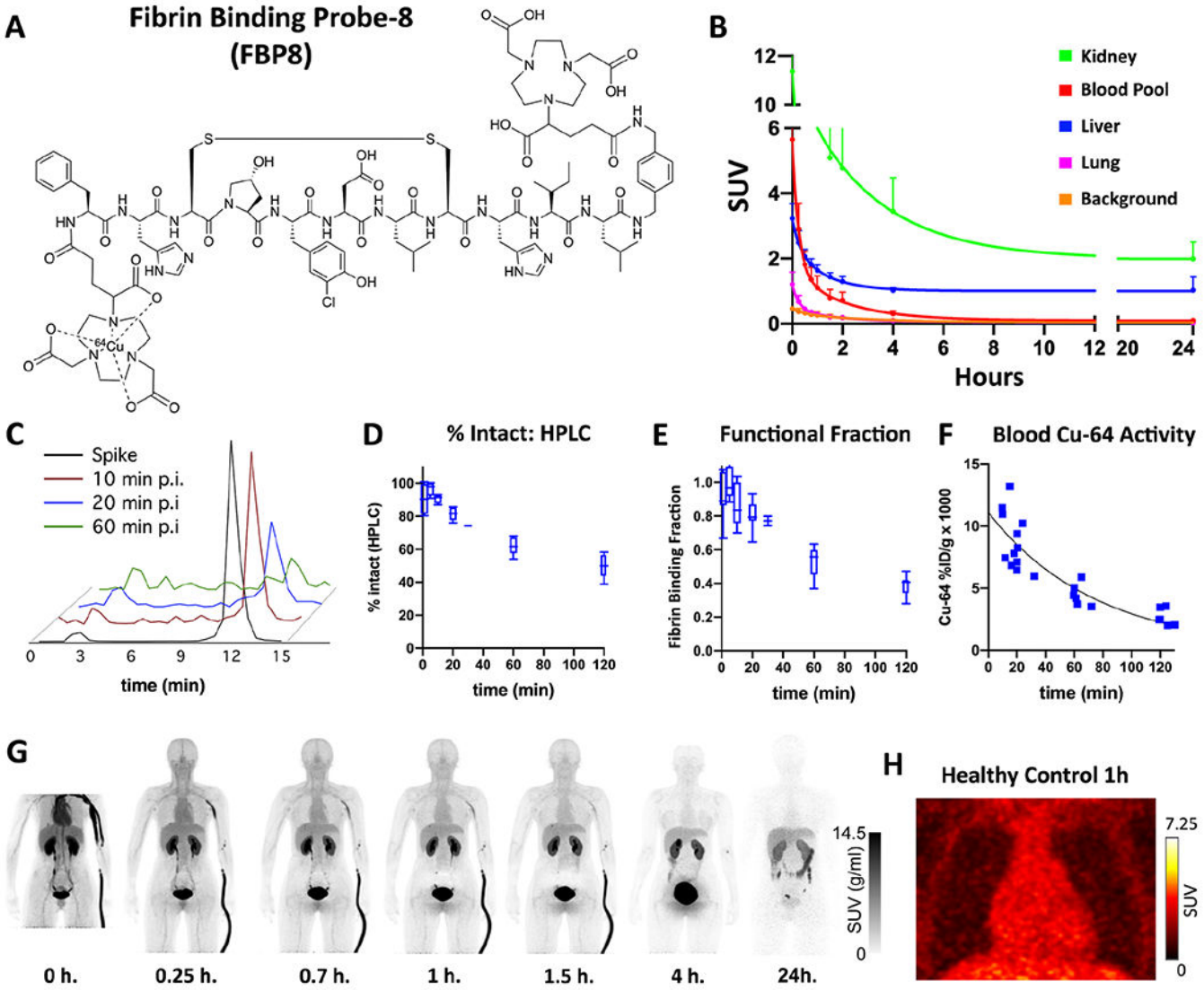

Figure 1. Structure and properties of ^{64}Cu-FBP8.

(A) The probe consists of a 6 amino-acid cyclic peptide with a high affinity for fibrin, conjugated to a ^{64}Cu-containing chelator (NODAGA). (B) Average time activity curves (TACs) from 5 healthy subjects, expressed as SUV (g/ml), show a relatively rapid reduction of the PET signal in the blood and lung, accompanied by renal and hepatic elimination. Image analysis of the blood pool showed that ^{64}Cu-FBP8 was eliminated from the blood in a bi-exponential manner typical of radiotracers with extracellular distribution and renal clearance, with an initial distribution phase (alpha $t_{1/2}$ = 6.9 ± 3.0 min) followed by an elimination phase (beta $t_{1/2}$ = 68 ± 2 min). (C-F) Chemical analysis of blood samples taken from healthy volunteers injected with [^{64}Cu]FBP8. (C) High Performance Liquid Chromatography (HPLC) of ^{64}Cu-containing moieties in the blood at various times postinjection shows that the majority of ^{64}Cu activity is intact [^{64}Cu]FBP8 which has a retention time of 12 minutes. (D) [^{64}Cu]FBP8 is stable in blood, with >60% of the probe still intact by HPLC one hour after injection. (E) Over 50% of the probe remains functional and able to bind fibrin 1 hour after injection. (F) The clearance of ^{64}Cu activity from the

blood, measured by venous blood sampling and expressed as %ID/g, indicates a one-hour blood elimination half-life (beta $t_{1/2}$ = 57 ± 7 min). (G-H) Biodistribution of [^{64}Cu]FBP8 in a healthy control subject shows a substantial reduction in the background thoracic signal within 1 hour of injection, and a near-complete loss of background by 4 hours. Elimination of the probe in the bladder and gallbladder is clearly seen. (H) Magnified view of the thorax at 1 hour showing no evidence of focal [^{64}Cu]FBP8 uptake in either the heart or lungs.

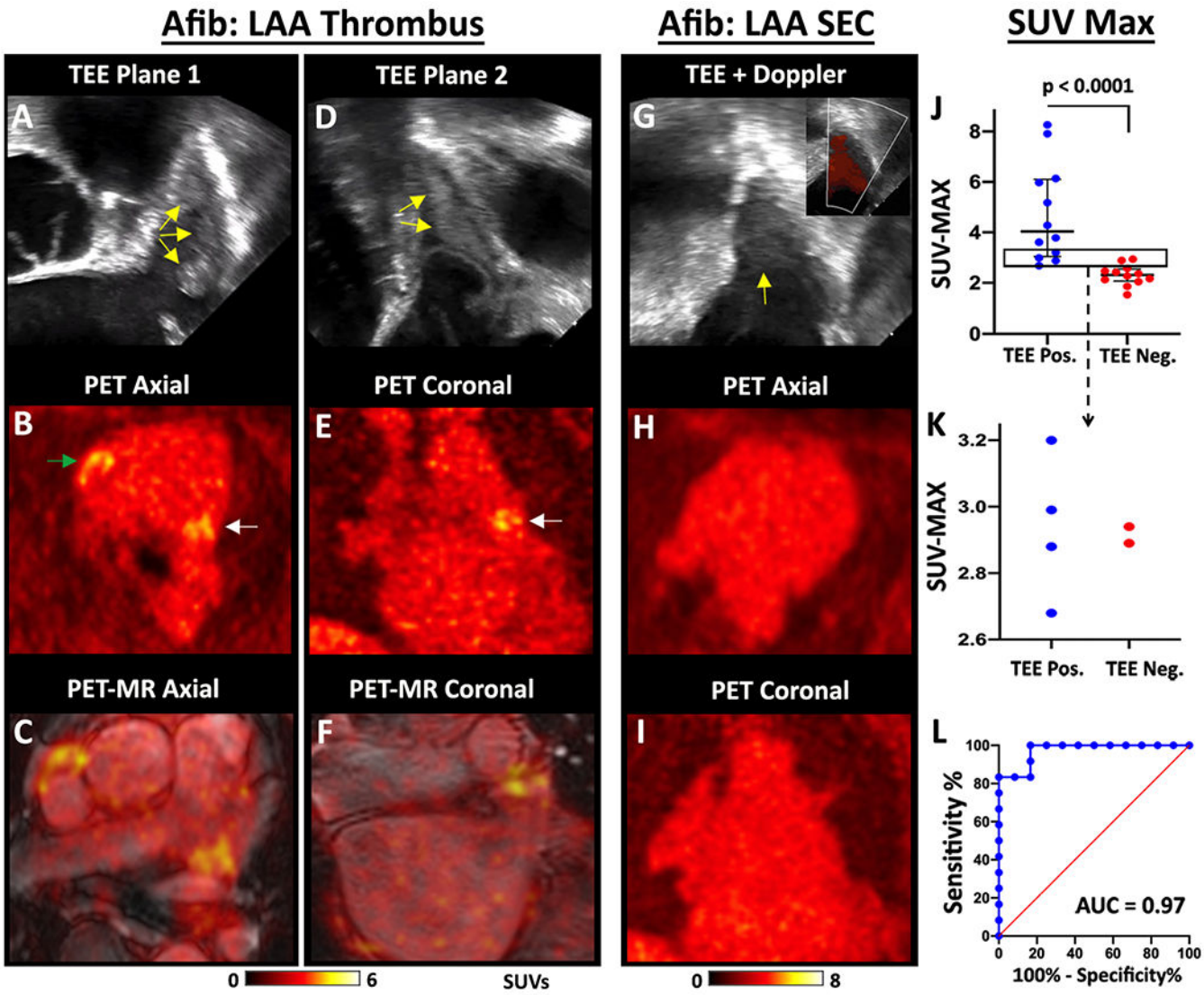

Figure 2. Detection of spontaneous thrombi in the LAA.

TEE, PET and fused PET/MRI images of a subject with multiple LAA thrombi are shown in two orthogonal planes, (A-C) and (D-F). The thrombi produce echogenic/bright foci (yellow arrows) on the TEE images (A, D). The PET (B, E) and PET/MRI (C, F) images reveal multiple foci of [^{64}Cu]FBP8 uptake in the LAA (white arrows) in both planes. In addition, thrombus is also identified in the RAA (green arrow). (G-I) [^{64}Cu]FBP8 does not accumulate in the LAA in a subject with spontaneous echo contrast (SEC) but no thrombus. (G) Echogenic signal is seen within the LAA (yellow arrow), but color Doppler (inset) reveals extensive flow consistent with SEC. No evidence of LAA thrombus is seen on the [^{64}Cu]FBP8 PET images in the axial (H) or coronal (I) views. (J-L) The maximum SUV value in the LAA (SUV_{MAX}) accurately distinguishes TEE positive and negative subjects. (J) SUV_{MAX} in the TEE positive subjects was significantly higher than the TEE negative subjects. (J-K) A SUV_{MAX} threshold of 2.6 correctly classified all (12/12) TEE positive subjects and 10/12 TEE negative subjects. The area in the rectangle in panel J is magnified in panel K and confirms that a SUV_{MAX} threshold of 2.6 produces no false

negative and only 2 false positive cases. (L) Receiver operating characteristic (ROC) curve demonstrates the robustness of [^{64}Cu]FBP8 SUV_{MAX} in distinguishing TEE positive and negative subjects, with an area under the curve (AUC) of 0.97.

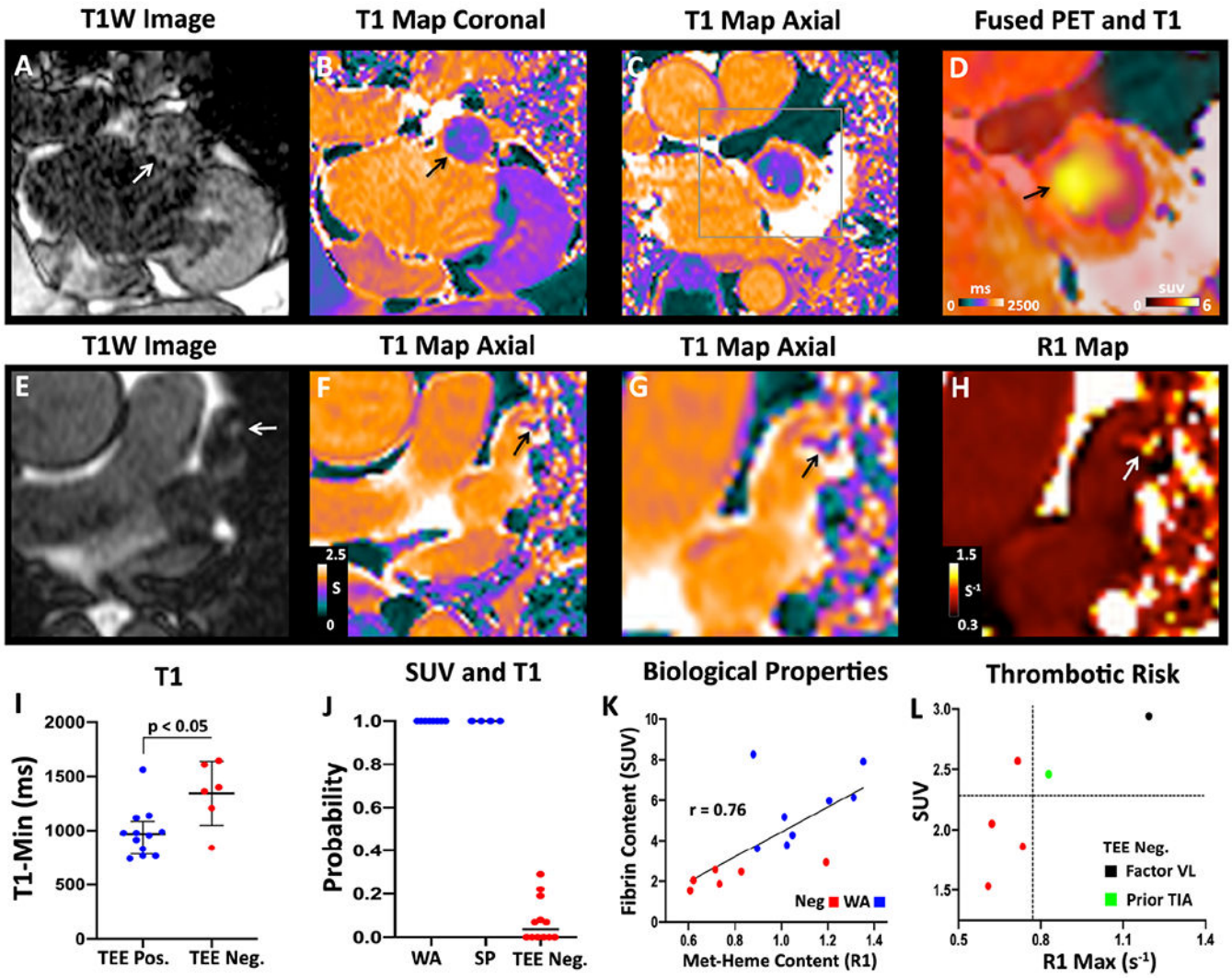

Figure 3. Integrated analysis of magnetic relaxation (T1) and SUV_{MAX} in the LAA.

(A-D) Subject with a LAA closure device. (A) T1-weighted image in the coronal plane showing a hyperintense region in the LAA (white arrow). (B) T1 map in the same view demonstrating low values (green-purple; black arrow) in the LAA, similar to the T1 of myocardium (purple) but far lower than the blood pool (orange). (C) Axial T1 map confirms the presence of short-T1 (paramagnetic) species in the LAA, consistent with methemoglobin (met-heme) accumulation in thrombus. (D) Magnified view of the axial T1map fused with the [^{64}Cu]FBP8 PET image demonstrates a high degree of the overlap between low T1 and high [^{64}Cu]FBP8 uptake. (E-H) Spontaneous LAA thrombus. (E) Axial T1W image showing a hypertintense focus (arrow) in the LAA. (F) Axial T1 map shows a focus of reduced T1 (arrow) in the LAA. (G) Magnified view of T1 map and short T1 focus (arrow). (H) Magnified view of R1 map (units s^{-1}). The thrombus in the LAA (arrow) has a high R1 value. (I) The minimum T1 value ($T1_{MIN}$) in the LAA is significantly shorter in the TEE positive than negative group. (J) Probability of having a LAA thrombus based on logistic regression of the z-scores for both SUV_{MAX} and $T1_{MIN}$. WA = Watchman, SP = spontaneous. (K) Biological properties of the LAA (fibrin and met-heme content) in those

with precisely aged recent thrombi (WA group) and no thrombi (Neg group). A strong correlation is seen between fibrin content (SUV_{MAX}) and met-heme content ($R1_{MAX}$ = $1/T1_{MIN}$). (L) Within the TEE negative group an association may be present between higher SUV and R1 values and thrombotic risk. Factor VL = Factor V Leiden.

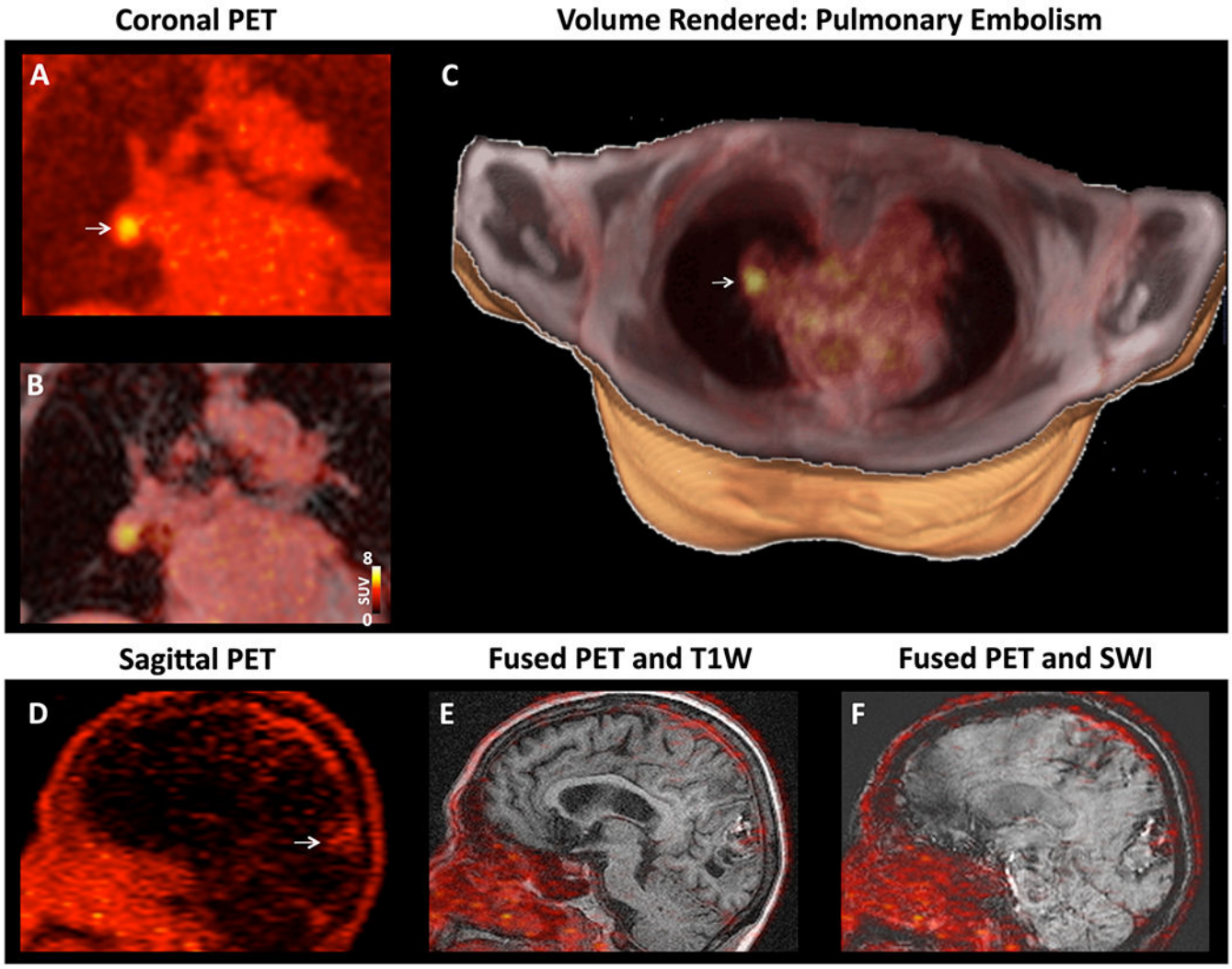

Figure 4. [^{64}Cu]FBP8 facilitates whole-body thrombus detection.

(A-C) Right pulmonary artery embolism in a subject with a spontaneous LAA thrombus. (A) Coronal PET image with a focus of high [^{64}Cu]FBP8 activity (arrow). (B) Fusion of the PET and Dixon water images reveals that the thrombus is located within a branch of the right pulmonary artery. (C) Volume rendered image showing the pulmonary embolism (arrow,) in the right lung. (D-F) TEE positive subject with a history of a large intracranial bleed. (D) Sagittal PET image, (E) fused PET and T1-weigted image and, (F) fused PET and susceptibility weighted image (SWI). The PET image shows that a low level of [^{64}Cu]FBP8 uptake persists at the site of the bleed (arrow).

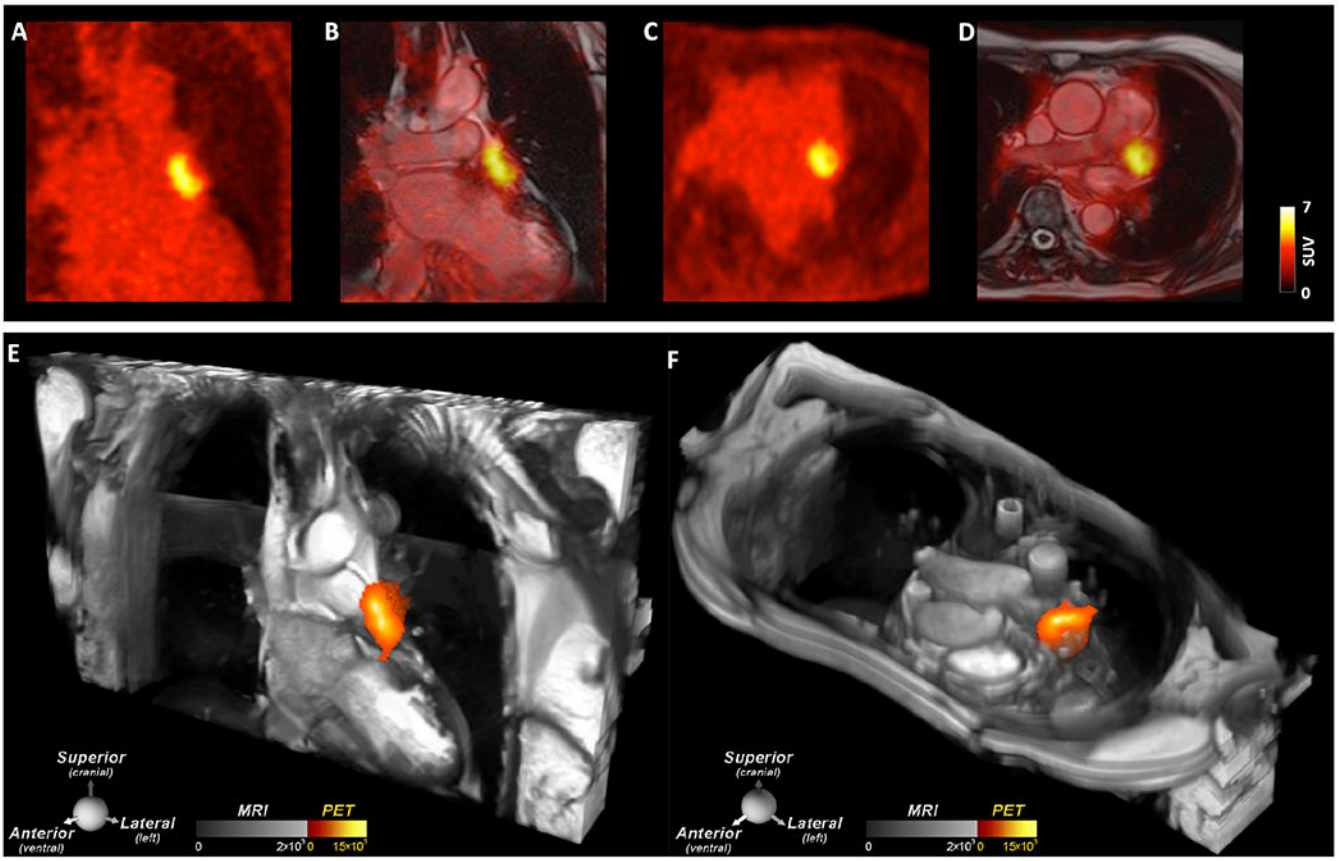

Central Illustration. Thrombus in the LAA induced by recent placement of a Watchman LAA closure device.

A large thrombus is seen in the LAA behind the device on (A, B) the coronal PET and PET/MRI images as well as (C, D) the axial PET and PET/MRI images. (E, F) 2D bSSFP cines stacks in the coronal and axial planes have been combined into a single 3D dataset and fused with the 3D PET data. In these multi-modal images the PET and MR data are both displayed in 3D, creating a volumetric depiction of the heart and the thrombus/[^{64}Cu]FBP8 containing LAA. Volume rendered images in the oblique coronal and axial planes confirm the presence of thrombus in the LAA. (A-F) The thrombus produced by the closure device is contained within the LAA, and no evidence of thrombus is seen elsewhere in the heart or thorax.

Table 1:

Characteristics of TEE Positive and TEE Negative Subjects

Characteristic	TEE Positive Patients (N = 12)	TEE Negative Patients (N = 12)	p-value
Age – yr			
Median	80	61	0.0035
Interquartile range	76-84	55-73	
Female sex – no. (%)	4 (33.3%)	4 (33.3%)	1.0000
CHA_2DS_2-VASc score			
Median	4.50	2.00	0.0101
Interquartile range	4.00-5.75	0.25-3.75	
GFR (ml/min) – mean ± sd	54.08 ± 14.23	65.55 ± 21.55	0.1542
Duration of atrial fibrillation - yr			
Median	1.33	0.62	0.1748
Interquartile range	0.63 - 2.74	0.07 - 1.32	
Type of atrial fibrillation			0.0996
Paroxysmal– no. (%)	3 (25.0%)	8 (66.7%)	
Persistent/Permanent– no. (%)	8 (66.7%)	4 (33.3%)	
Unspecified– no. (%)	1 (8.3%)	0 (0%)	
Current smoking status – no. (%)	0 (0%)	1 (8.3%)	1.0000
Concurrent diagnosis of hypertension – no. (%)	11 (91.7%)	8 (66.7%)	0.3168
Concurrent diagnosis of diabetes – no. (%)	5 (41.7%)	0 (0%)	0.0373
Prior stroke, TIA, or thromboembolism – no. (%)	5 (41.7%)	1 (8.3%)	0.1550
Hypercoagulability – no. (%)	0 (0%)	1 (8.3%)	1.0000
Anticoagulation status			0.2174
DOAC – no. (%)	9 (75.0%)	12 (91.7%)	
Warfarin – no. (%)	2 (16.7%)	0 (0%)	
Warfarin INR			
Median	3.30		
Interquartile range	3.25 - 3.35		
None – no. (%)	1 (8.3%)	0 (0%)	
ASA only – no. (%)	1 (8.3%)	0 (0%)	1.0000
Antiplatelet only – no. (%)	0 (0%)	0 (0%)	1.0000
Dual Rx (anticoagulation + ASA) – no. (%)	8 (66.7%)	3 (25%)	0.0995
Triple Rx (anticoagulation + ASA + antiplatelet) – no. (%)	2 (16.7%)	1 (8.3%)	1.0000
No. of days from qualifying TEE to imaging			
Median	9.50	11.00	0.4305
Interquartile range	5.00-12.00	8.00-12.75	
Previous Watchman device placement – no. (%)	8 (66.7%)	0 (0%)	
LAA Emptying Velocity (cm/s)			

Characteristic	TEE Positive Patients (N = 12)	TEE Negative Patients (N = 12)	p-value
Median	14.00	35.50	0.1134
Interquartile range	11.00-64.50	19.50-52.75	
LA Volume Index (ml/m^2) – mean ± sd	44.95 ± 12.65	36.79 ± 13.34	0.1680